Dyes and Pigments 161 (2019) 188–196

Contents lists available at ScienceDirect

Dyes and Pigments

journal homepage: www.elsevier.com/locate/dyepig

Oligo(ethylene oxide) chains in fluorene bridge units of perylenediimide dimers as an efficient strategy for improving the photovoltaic performance in organic solar cells

Joana Farinhas[a], Desiré Molina[b], Ana Olcina[b], Cristiana Costa[a], Luís Alcácer[a], Fernando Fernández-Lázaro[b], Ángela Sastre-Santos[b,**], Ana Charas[a,*]

[a] Instituto de Telecomunicações, Instituto Superior Técnico, Av. Rovisco Pais 1, P-1049-001, Lisboa, Portugal
[b] Área de Química Orgánica, Instituto de Bioingeniería, Universidad Miguel Hernández, Avda. de la Universidad s/n, 03203, Elche, Spain

ARTICLE INFO

Keywords:
Perylenediimide
Organic solar cells
Ethylene oxide

ABSTRACT

Perylenediimides (PDIs) are among the most promising non-fullerene electron-acceptors for applications in organic photovoltaics (PV), providing a large scope for structural modifications. PDI-based dimers have shown the highest performances in PV devices owing to their characteristic twisted conformations that reduce their tendency to form large aggregates which are detrimental for PV operation. In this work, two fluorene-bridged perylenediimide (PDI) dimers with oligo(ethylene oxide) or alkyl chains anchored to the C9 position of the fluorene unit were synthesized and investigated in solution-processed organic bulk heterojunction (BHJ) photovoltaic cells as electron acceptors. The PDI dimer substituted with oligo(ethylene oxide) chains resulted in improved power conversion efficiencies (in 20%–53%) in solution processed bulk heterojunction (BHJ) cells with two different polymer donors, PTB7 and PffBT4T-2OD. Nevertheless, the replacement of alkyl chains by oligo(ethylene oxide) chains did not significantly affect the geometric characteristics of the PDI dimers and the optical and electrochemical properties were only marginally modified. Increased exciton dissociation and enhanced charge transport derived from a more densely packed π-π stacking in the solid state caused by ethylene oxide groups are pointed out as possible causes for the improved PV performance. The influence of 1,8-diiodooctane as solvent additive in the blend films was also investigated and allowed to further increase the efficiencies of the cells with PTB7. Overall, the results show that the simple replacement of alkyl chains by oligo (ethylene oxide) chains in PDI dimers is an efficient way to improve the PV performance without compromising the optoelectronic properties of the PDI acceptor.

1. Introduction

Photovoltaic cells based on organic semiconducting materials represent a potential renewable energy technology due to their advantageous characteristics, such as light weight, mechanical flexibility and easy large-area fabrication involving low-cost solution processing [1–4]. The most efficient organic solar cells (OSCs) have already demonstrated relatively high power conversion-efficiencies (PCEs), in the range of 10–13% for single junction cells [5–7]. The improvements on cells performance resulted mainly from the optimization of the active layer morphology [6] and noteworthy advances on materials design focusing on the broadening of the optical absorption spectrum, increasing the hole mobility and tuning the electronic frontier energy levels [5–7]. Although significant progresses recently occurred on the acceptors side, leading to efficiencies surpassing 13% for molten ring electron acceptors (ITIC derivatives) [5], almost all the efficient OSCs contain soluble fullerene derivatives ([6,6]-phenyl-$C_{61/71}$-butyric acid methyl ester, $PC_{61}BM$ and $PC_{71}BM$, respectively) due to their high electron mobilities [8] and very efficient charge separation in combination with several donors [9,10]. However, fullerenes present inherent drawbacks to further raising of OSCs efficiencies due to their weak and narrow solar absorption spectra, photo-instability in air conditions [11] and difficult functionalization to tune their optical gaps and energy levels over a wide energy range [12].

Perylenediimide derivatives (PDIs) are among the most investigated classes of non-fullerene acceptors, owing to their low LUMO levels,

* Corresponding author.
** Corresponding author.
E-mail addresses: asastre@umh.es (Á. Sastre-Santos), ana.charas@lx.it.pt (A. Charas).

https://doi.org/10.1016/j.dyepig.2018.09.051
Received 26 June 2018; Received in revised form 5 September 2018; Accepted 19 September 2018
Available online 22 September 2018
0143-7208/

strong absorption of the solar spectrum and good thermal, chemical, and photo-stabilities [13–16]. Also, they possess a rigid and planar π-conjugated core which favours ordered molecular packing and facilitates charge transport. This feature allows PDIs to be among the *n*-type organic semiconductors with highest electron mobilities in field effect transistors [17]. In OSCs, PDI-based molecules usually result in moderate performances due to the formation of large aggregates (promoted by intermolecular π-π stacking), where the large pathways to the donor/acceptor interfaces cause geminate recombination of excitons and reduce free charges' generation. Recently, Y. Zhong and *co*-workers [13] reported on helical PDIs possessing nonplanar structures which hinder aggregates formation and result in mesh-like networks incorporating the donor that improve both exciton dissociation and charge transport. PCEs of 7.9–8.3% were found for optimized devices with such PDIs and the donor polymer PTB7-Th. PDI-based dimers with strongly twisted configurations and with sulphur, selenium [14,18] or nitrogen-alkyl groups [19] in the perylene core also exhibited PCEs in the range of 7–8.5% with the polymers PDBT-T1 or P3TEA after blend optimization with additives. Noteworthy, bridging two PDI units through the bay positions with certain spacers (thiophene, spirobifluorene, phenylene, etc.) has resulted in PDI dimers with nonplanar conformations that impede large aggregates formation in blend films. Lately, this molecular design has been extensively explored in many works and has resulted in several well-performing PV layers [20–24]. Apart from the mentioned strategies to alter the PDIs' geometry and consequently intermolecular packing, other structural modifications, as the nature of the side chains anchored to the conjugated backbones are determinant to the device efficiency. In fact, in BHJ solution processed cells, the charge photogeneration processes strongly depend on the morphology of the active layer which in turn is predetermined by the miscibility between the donor and the acceptor. Nevertheless, the role of the solubilizing groups of PDIs in solution-processed PVs has been poorly explored, being limited to studies involving alkyl chains [23,25].

In this work, we investigate the effect of solubilizing groups in perylenediimide dimers with fluorene bridge units substituted with either *n*-octyl chains (**PDI-F8**) or linear chains with two ethylene oxide groups (**PDI-Feo**) (Scheme 1) in BHJ PV cells performance. The effect of oligo(ethylene oxide) (EO) side chains is of special relevance for solution-processed optoelectronic devices since they can increase the solubility in environmentally friendly solvents (hydrophilic solvents as water and ethanol) and prompt "greener" device fabrication, while their non-ionic nature does not exacerbate trapping for the generated charges. In addition to enhanced polarity, EO chains have smaller rotation barriers of O-CH_2 bonds than CH_2-CH_2 bonds in alkyl chains [26], this causing less steric effects for rotation and higher flexibility [27,28]. Indeed, some recent works demonstrated the beneficial effect of side chains with ethylene oxide groups in polymer donors in OSCs. Y. Chen et al. synthesized a conjugated polymer donor with triethylene glycol monoether (TEG) side chains which could be processed from solvents of low toxicity yielding slightly higher efficiencies than those of the corresponding devices processed with chlorinated solvents [29]. Also, it was shown that side chains with EO functionality in polymer donors can induce large dipole moments that may favour exciton dissociation and lead to increased photogenerated currents [30]. X. Chen et al. synthesized diketopyrrolopyrrole-based conjugated polymers bearing branched OE side chains exhibiting higher hole mobility, red-shifted absorption, higher dielectric constant and enhanced OSC performance than the analogous with branched alkyl side chains [31]. In the present study, we show the comparison of the structural, optical, and electrochemical properties of two new PDI dimers only differing on the solubilizing chains of the bridge unit and a beneficial effect of EO chains in relation to alkyl chains on the PV performance in OSCs. The obtained results provide novel guidelines for the molecular design of non-fullerene electron-acceptors with advantageous properties in OSCs.

2. Experimental section

2.1. Materials and synthesis

PffBT4T-2OD (Poly[(5,6-difluoro-2,1,3-benzothiadiazol-4,7-diyl)-*alt*-(3,3‴-di(2-octyldodecyl)-2,2′; 5′,2″; 5″,2‴-quaterthiophen-5,5‴-diyl)]) and PTB7 (Poly[[4,8-bis[(2-ethylhexyl)oxy]benzo[1,2-b:4,5-b']dithiophene-2,6-diyl][3-fluoro-2-[(2-ethylhexyl)carbonyl]thieno[3,4-b]thiophenediyl]]) were purchased from Ossila. All the solvents used for synthesis were dried according to standard methods. All the reactions were carried out under inert atmosphere (N_2). Unless otherwise stated, all the reagents were purchased from commercial suppliers and used as received. 2,7-bis(4,4,5,5-tetramethyl-1,3,2-dioxaborolan-2-yl)-9,9-dioctyl-fluorene (**3**) was prepared from fluorene following a modified procedure of that reported in Ref. [32]. NMR spectra were recorded at 25 °C using a Bruker AC300 spectrometer. High resolution mass spectra were obtained from a Bruker Microflex LRF20 matrix-assisted laser desorption/ionization time of flight (MALDI-TOF) using dithranol as matrix. IR spectra were measured with a Nicolet Impact

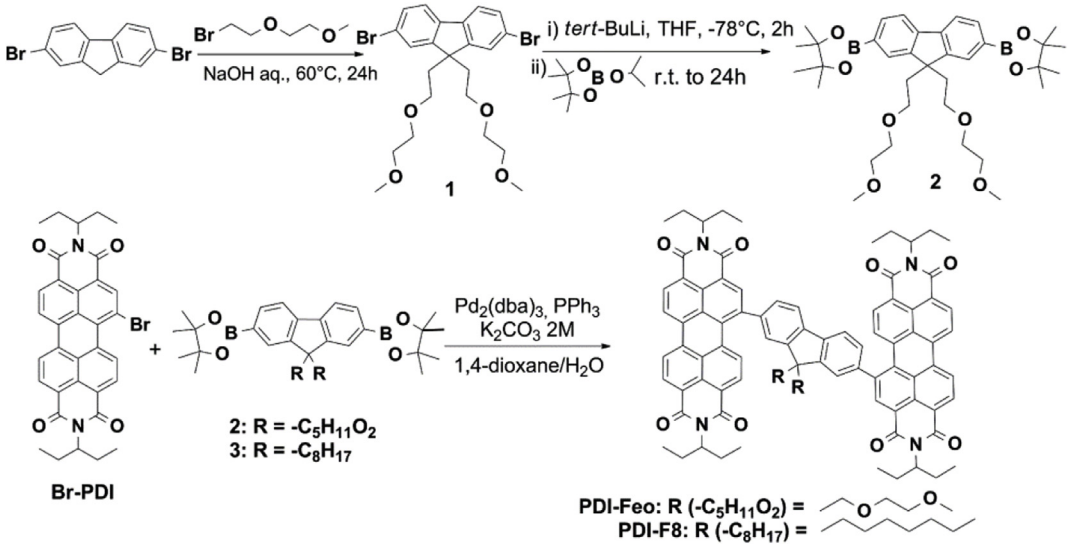

Scheme 1. Synthetic strategies. Synthesis of the intermediate fluorene monomer with ethylene oxide side chains and of the two PDI dimers with either *n*-octyl (**PDI-F8**) or oligo(ethylene oxide) side chains (**PDI-Feo**).

400D spectrophotometer. The solvents for spectroscopic studies were of spectroscopic grade and used as received.

2.1.1. 2,7-dibromo-9,9-bis(2-(2-methoxyethoxy)ethyl)-9H-fluorene (1)

4.0 g (12.3 mmol) of 2,7-dibromofluorene were added to a solution of 21 ml of NaOH aq. (50%) and 1.28 g (4.0 mmol) of tetrabutylammonium bromide, under stirring, at room temperature. The red suspension was heated to 60 °C for 15 min and 1-bromo-2-(2-methoxyethoxy)ethane (2.61 ml, 18.5 mmol) was added drop wise. After stirring for 24 h at 60 °C, the product was extracted with a mixture of THF/Et_2O (50:50, v/v) and the organic phase was washed with H_2O until neutral pH, and dried over Na_2SO_4. After evaporating the solvent, a yellowish oil was obtained and this was submitted to chromatography on silica using hexane/EtOAc (1/1, v/v) as eluent yielding 3.73 g (6.0 mmol) of pure product as a pale-yellow oil. Yield, 49%. ^{1}H NMR (300 MHz, $CDCl_3$, *d*, ppm): 7.44–7.56 (m, 6H), 3.27–3.33 (m, 10H), 3.15–3.22 (m, 4H), 2.77 (t, J = 7.4 Hz, 4H), 2.36 (t, J = 7.4 Hz, 4H). Anal. Calcd. for $C_{23}H_{28}Br_2O_4$ (%): C, 52.29; H, 5.34. Found: C, 51.80; H, 5.51.

2.1.2. 2,7-Bis(4,4,5,5-tetramethyl-1,3,2-dioxaborolan-2-yl)-9,9-bis(2-(2-methoxyethoxy)ethyl)-9H-fluorene (2)

To a solution of 731 mg (1.38 mmol) of **1** in 30 ml of THF, under stirring, at −78 °C, 3.6 ml of *tert*-BuLi (1.7 M in pentane) were added drop wise, under N_2. After 2 h at −78 °C, the reddish suspension was warmed to 0 °C for 15 min and then it was cooled again to −78 °C. At this temperature, 1.72 g (8.3 mmol) of 2-isopropoxy-4,4,5,5-tetramethyl-1,3,2- dioxaborolane were added under N_2 and the reaction warmed until room temperature and was stirred for 24 h. After this period, water was added and the phases were separated. The aqueous phase was extracted with Et_2O and the organic phase was washed with brine and dried over anhydrous Na_2SO_4. After evaporating the solvent, a viscous colorless oil was obtained which yielded 794 mg (1.28 mmol) of a white solid (pure product) by recrystallization from ethanol. Yield, 93%. ^{1}H NMR (300 MHz, CDCl3, *d*, ppm): 7.85 (s, 2H), 7.80 (d, J = 7.6 Hz, 2H), 7.70 (d, J = 7.4 Hz, 2H), 3.23–3.34 (m, 10H), 3.11–3.18 (m, 4H), 2.62–2.73 (m, 4H), 2.42–2.52 (m, 4H), 1.85 (dt, J = 6.2, 3.3 Hz, 4H), 1.39 (s, 24H). Anal. Calcd. for $C_{35}H_{52}B_2O_8$ (%):C, 67.54; H, 8.42. Found: C, 67.08; H, 8.67.

2.1.3. PDI-F8

To a degassed solution of 50 mg (0.08 mmol) of brominated PDI (**Br-PDI)** [33]. 0.17 mmol of 9,9-dioctyl fluorene diboronic ester (**2**), 30 mg (0.03 mmol) of $Pd_2(dba)_3$ and 69 mg (0.26 mmol) of triphenylphosphine in 2.2 ml of degassed 1,2-dioxane, 0.67 ml of a 2M degassed aqueous solution of K_2CO_3 were injected. This mixture was heated at 85 °C for 46 h under argon. The crude was washed with methanol and purified by silica gel column chromatography using chloroform/ethyl acetate (20:1) as eluent. The pure compound was obtained as a copper-colored solid. Yield, 51%. ^{1}H NMR (300 MHz, $C_2D_2Cl_4$, *d*, ppm): 8.73–8.67 (m, 10H), 8.20 (d, J = 8.3 Hz, 1H), 8.07–7.90 (m, 5H), 7.59–7.49 (m, 4H), 5.08 (m, 4H), 2.26 (m, 8H), 1.98 (m, 12), 1.12–0.64 (m, 54H). ^{13}C NMR (75 MHz, $C_2D_2Cl_4$, *d*, ppm): 164.4, 164.2, 164.1, 153.4, 153.3, 142.3, 141.8 (x2), 140.9 (x2), 135.0 (x3), 134.9 (x2), 134.6, 134.5, 132.9, 132.8, 129.2 (x2), 128.6, 128.1, 127.6 (x2), 123.8, 122.8, 122.6, 57.8 (x2), 57.6 (x3), 56.1, 56.0, 31.9, 29.4, 25.2, 25.1, 22.8, 22.7, 22.6, 14.3, 14.2 (x2), 11.6 (x2), 11.5. UV-Vis (CH_2Cl_2) λ_{max}/nm (log ε): 320 (4.63), 466 (4.59), 530 (4.77). MALDI-TOF (*m/z*): M^- calcd. $C_{97}H_{98}N_4O_8$, 1447.737; found, 1447.767. IR (neat, cm^{-1}): 2963 (ν_A CH_3), 2929 (ν_A CH_2), 2875 (ν_S CH_3), 2854 (ν_S CH_2), 1699, 1658, 1593, 1562 (C=O), 1507, 1460 (C=C aromatic), 1405, 1335 (C-N), 1249, 1199.

2.1.4. PDI-Feo

To a degassed solution of 200 mg (0.33 mmol) of **Br-PDI** [31], 109 mg (0.17 mmol) of **3**, 30 mg (0.033 mmol) of Pd_2dba_3 and 69 mg (0.26 mmol) of PPh_3 in 2.2 ml of 1,2-dioxane, 0.7 ml of a 2M K_2CO_3 degassed solution was injected. After stirring for five minutes at room temperature, the reaction was heated at 80 °C for 16 h under argon, maintaining vigorous agitation. The crude was purified by silica gel column chromatography using CH_2Cl_2/THF (20:1) as eluent. The compound was obtained as metallic red powder. Yield, 50%. ^{1}H NMR (300 MHz, $CDCl_3$, *d*, ppm): 8.75–8.59 (m, 10H), 8.20–7.94 (m, 6H), 7.59–7.51 (m, 4H), 5.13–5.01 (m, 4H), 3.47–3.17 (m, 14H), 3.05–2.86 (m, 4H), 2.48–2.15 (m, 12H), 1.98–1.94 (m, 8H), 1.04–0.87 (m, 24H). ^{13}C NMR (75 MHz, $CDCl_3$ *d*, ppm): *d* 164.2, 164.1, 164.0, 151.6, 151.5, 142.6 (x2), 141.7, 140.0, 136.2, 134.8, 134.7, 134.4 (x2), 132.5, 131.2, 131.1, 129.9, 129.8, 129.3, 128.7, 128.4 (x2), 128.0, 127.6, 123.6, 123.1, 123.0, 122.8, 122.5 (x2), 72.0, 71.9, 71.7, 70.7, 70.3, 70.0, 67.4 (x2), 67.1, 66.9, 58.9 (x2), 58.8, 57.8, 57.6, 52.2, 52.1, 40.0, 39.8, 39.7, 25.1, 11.4. UV-vis (CH_2Cl_2) λ_{max}/nm (log ε): 229 (5.18), 532 (4.81); MALDI-TOF (*m/z*): $[M+H]^+$ calcd. $C_{91}H_{86}N_4O_{12}$, 1428.6348; found, 1428.6060; IR (neat, cm^{-1}): 2962 (ν_A CH_3), 2932 (ν_A CH_2), 2874 (ν_S CH_3), 1698, 1656, 1591, (C=O), 1460 (C=C aromatic), 1403, 1332 (C-N), 1248, 1194.

2.2. Measurements

UV-Vis spectra were measured with a Helios Gamma spectrophotometer. Cyclic voltammetry measurements were performed in 0.1M tetrabutylammonium hexafluorophosphate dichloromethane solution as support electrolyte, a graphite working electrode, a Ag/Ag^+ reference electrode, and platinum counter electrode. AFM studies were performed on a Nano Observer from Concept Scientific Instruments (Les Ulis, France), operating in noncontact mode, with cantilevers having a resonance frequency between 200 and 400 kHz and silicon probes with tip radius smaller than 10 nm. All images were obtained with 256 × 256 pixels resolution and processed using Gwyddion (version 2.26) software. Current-voltage (I-V) characteristics of the cells were measured under inert atmosphere (N_2) illuminating with a solar simulator (Oriel Sol 3A, 69920, Newport) with simulated AM 1.5G illumination at 81–85 mW cm^{-2}. The light intensity was determined with a calibrated solar cell. External quantum efficiency (EQE) spectra were obtained under short-circuit conditions, using a homemade system with a halogen lamp as light source.

2.3. Device fabrication

The OSCs were fabricated onto glass/ITO (100 nm) substrates which were washed sequentially with distilled water with a non-ionic detergent, distilled water, acetone (HPLC grade), and isopropyl alcohol (HPLC grade) under ultrasounds. The substrates were then treated with UV-oxygen plasma for 3 min. A 40 nm thick layer of PEDOT:PSS (poly (3,4-ethylene dioxythiophene:polystyrene sulfonic acid) was then spin-coated on top from an aqueous dispersion (Heraeus Clevios PVP.Al 4083) and the substrates were dried at 125 °C for 10 min. The blend solutions were prepared by stirring the polymer:PDI mixture in the appropriate ratio in chlorobenzene. Blend solutions of PTB7:**PDI-F8** and PTB7:**PDI-Feo** were prepared with concentrations of 30 mg/ml and 20 mg/ml, respectively, and the solutions were stirred on a hot plate at *ca.* 100 °C, overnight. In the case of devices with PTB7, the solutions were spin coated on ITO/PEDOT:PSS substrates in a nitrogen-filled glove box at ambient temperature (1500 rpm, 60 s). For the devices with PffBT4T-2OD the solutions were stirred on a hot plate at ca. 110 °C for 3 h prior to spin coating and they were spin-coated on pre-heated ITO/PEDOT:PSS substrates on a hot plate at 110 °C in a nitrogen-filled glove box (800 rpm, 15 s followed by 1100 rpm, 45 s) and the films were annealed at 110 °C for 5 min. The blend films were then transferred to the vacuum chamber for thermal evaporation of the top electrode. 20 nm of calcium followed by 100 nm of aluminum were evaporated at a base pressure below 2×10^{-6} mbar, defining a solar cell active area of 0.24 cm^2. At least 16 devices were prepared for each

condition.

3. Results and discussion

3.1. Synthesis

The two new PDI dimers, **PDI-F8** and **PDI-Feo** (Scheme 1), were designed with short alkyl groups at the N-position, in order that solubility is mainly determined by the longer chains in the fluorene unit. **PDI-F8** and **PDI-Feo** were synthetized in good yields by Suzuki-Miyaura coupling reactions of the 1-bromo substituted PDI (Br-PDI) with the corresponding fluorene diboronic ester in sealed tubes and under pressure. The fluorene diboronic ester functionalized with 2-(2-methoxyethoxy)ethyl units **(2)** was prepared from 2,7-dibromofluorene in two steps with 46% global yield according to Scheme 1. The new dimers were fully characterised by ^{1}H NMR, ^{13}C NMR, UV-Vis and FT-IR spectroscopies, and HR-MALDI-TOF mass spectrometry (see Section 2.1. and Appendix A).

3.2. Theoretical calculations

To assess to the optimized geometric configurations of the PDI dimers, theoretical calculations were performed employing the density functional theory (DFT) at the B3LYP/6- 31G(d)* level using quantum chemical software (Spartan, Wave Function Inc. CA). As shown in Fig. 1, both molecules show a very twisted conformation regarding the angle between the PDI sub-units and the fluorene unit. The dihedral angles between the naphthalimide which is directly connected to the fluorene unit and the fluorene are very similar for both dimers, being 56.86° and 52.76° for **PDI-F8** and 66.14° and 57.76° for **PDI-Feo**. In both, the PDI sub-units lie almost in the same plane, being the differences between those dihedral angles of 4.10° (**PDI-F8**) and 8.38° (**PDI-Feo**). Thus, it can be concluded that the presence of ethylene oxide groups results on slightly larger torsion between the PDI planes. As shown in Fig. S7 of Appendix A, the HOMO and LUMO distributions are analogous for the two PDI dimers. In both dimers, the LUMO is located mainly in the PDI sub-units, with negligible contribution from the central fluorene unit. In contrast, the fluorene unit contributes strongly to the HOMO. As expected, the side chains anchored to the imide groups and to the fluorene bridge unit do not contribute to the frontier molecular orbitals.

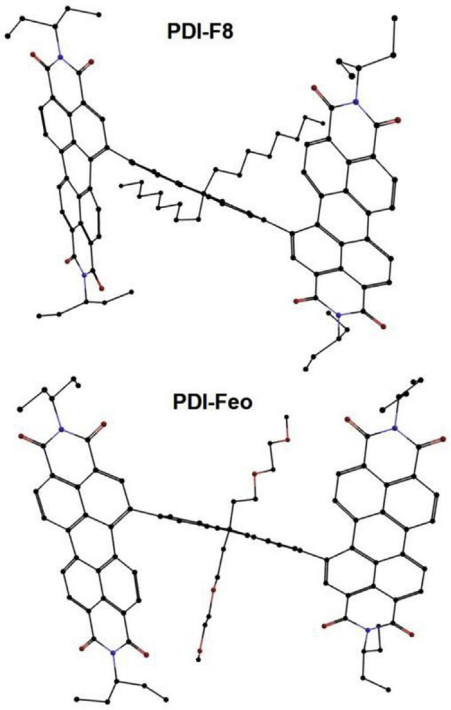

Fig. 1. Optimal geometries for the PDI dimers (side view) obtained from DFT calculations. Hydrogens have been removed for clarity. Black, carbon; red, oxygen; blue, nitrogen. (For interpretation of the references to color in this figure legend, the reader is referred to the Web version of this article.)

3.3. Optical and electrochemical properties

UV-Vis absorption measurements for the PDI dimers were obtained in dichloromethane (DCM) solution and in spin cast thin films prepared from concentrated chlorobenzene solutions (Table 1 and Fig. 2). In DCM solution, both dimers absorb strongly and with very similar molar extinction coefficients in the wavelength range from 400 to 600 nm with maxima located at 530 nm (Fig. S8 in Appendix A). The similarity between the absorption spectra of both PDIs in solution indicates that the EO side chains in the fluorene unit do not alter the electronic structure of the conjugated backbones when the chromophores are isolated (in diluted solution). In films, both PDIs absorb in the same optical range and the main peaks are kept at similar positions with respect to the spectra in solution, indicating weak intermolecular aggregation in the solid state. This low tendency to aggregate in solid state can be due to the non-planar structure of the PDIs as previewed by DFT calculations. Nevertheless, the onset wavelength of absorption of **PDI-Feo** (625 nm) is a little larger than that of **PDI-F8**, thus resulting in a little shorter optical bandgap ($E_{g,opt}$). Likewise, in film, the emission band of **PDI-Feo** extends to lower energies than that of **PDI-F8**. These shifts to lower energies in both absorption and emission band edges found for **PDI-Feo** in relation to those of **PDI-F8** indicate larger delocalization of the π states in the solid state for the **PDI-Feo** case. Red shifts in absorption were also found for conjugated polymers with fluorene units with oligo(ethylene oxide) chains in the C9 position when compared with analogous polymers with alkyl chains [34]. In the case of such polymers, the red shifts were analyzed with grazing incidence X-ray diffraction (GI-XRD) measurements and showed smaller π-π stacking distances in the solid state for the polymers with EO side chains. We propose that, similarly, the EO side chains in **PDI-Feo** favour a better stacking in solid film compared to *n*-octyl chains and that can be at the origin of the observed modification of the optical spectra. Fig. 2 also shows the absorption of the two polymer donors, chosen for this study, PffBT4T-2OD [35] and PTB7 [36].

As observed, the absorption bands of the PDI dimers are complementary to those of the polymer donors providing a wide spectral coverage over the visible spectrum, from 400 to 750 nm, for both investigated donor-acceptor systems.

Cyclic voltammetry (CV) was used to estimate the highest occupied molecular orbital (HOMO) and lowest unoccupied molecular orbital (LUMO) for the PDI dimers (Table 1). The redox couple ferrocene/ferricenium ion (Fc/Fc^{+}) was used as external standard. Considering that the reference level for ferrocene is 4.8 eV below the vacuum, the energy positions of the HOMO and LUMO levels were estimated from the onset values for the reduction and oxidation potentials through the equations: LUMO = -($E_{red,onset}$ (*vs.* Fc/Fc^{+}) + 4.80 eV) and HOMO = -($E_{ox,onset}$ (*vs.* Fc/Fc^{+}) + 4.80 eV). As shown in Fig. S9 (Appendix A), both dimers exhibit similar redox processes, indicating that the presence of ethylene oxide groups instead of alkyl chains do not significantly influence their frontier energy levels when measured in solution, as expected. The obtained values for the HOMO and LUMO energies are slightly raised than those reported for the PDI monomer (HOMO/LUMO = −5.99 eV/-3.74 eV) [21] and close to others reported for PDI dimers with aromatic bridge units, as vinylene units (HOMO/LUMO = −5.88 eV/-3.83 eV) [37] and 9,9′-spirobifluorene units (−5.71 eV/-3.71 eV) [21].

Table 1
Optical and electrochemical properties of **PDI-F8** and **PDI-Feo**.

PDI dimer	λ_{abs} [nm] soln.	λ_{abs} [nm] film	λ_{em} [nm] film	$E_{g,opt}$[a] [eV]	HOMO [eV]	LUMO [eV]
PDI-F8	466, 501, 530	474, 495, 534	689	2.00	−5.80[b] (−5.70)[c]	−3.80[b] (−3.41)[c]
PDI-Feo	464, 503, 530	473, 494, 532	688	1.98	−5.60[b] (−5.78)[c]	−3.78[b] (−3.40)[c]

[a] Optical bandgap estimated from the absorption edge of the thin film.
[b] Estimated by cyclic voltammetry.
[c] DFT calculated values in parentheses.

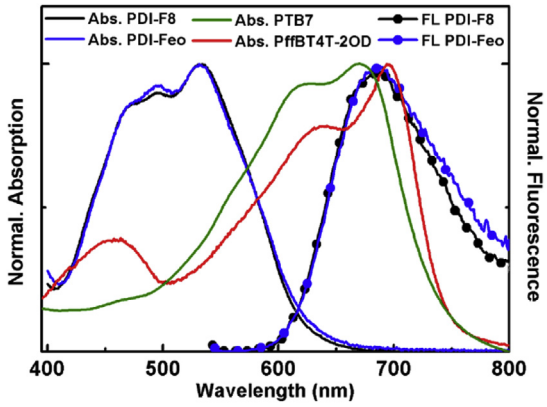

Fig. 2. UV-Vis absorption and fluorescence spectra (λexc. = 530 nm) of the PDI dimers and absorption of PTB7 and PffBT4T-2OD deposited as spin cast films over quartz substrates.

3.4. Organic solar cells

To assess the photovoltaic properties of the two PDI dimers, they were applied as the electron-acceptor in solution-processed BHJ OSCs. To better evaluate the PV performance of the PDIs in BHJ blends, two polymers with significant structural dissimilarities (Fig. 3), PffBT4T-2OD [35] and PTB7 [36], were chosen as polymer donors. The general device structure was glass/ITO/PEDOT:PSS/polymer:PDI dimer/Ca/Al. The active layers (AL) were prepared by spin-coating the blend solutions in chlorobenzene (see Experimental section for details). Two polymer:PDI ratios, 1:1 and 1:1.5 (wt/wt), were tested for PffBT4T-2OD:PDI based cells and the 1:1 composition was tested for PTB7:PDI based cells. 1,8-Diiodooctane (DIO) was tested as additive in the solvent in 1% and 3% (%vol) in PTB7:PDI blends. For PffBT4T-2OD-based blends, the presence of DIO led to very heterogeneous films that resulted in very poor PV performances. The active layers (AL) thicknesses were measured with a profilometer. Films from blends with PffBT4T-2OD displayed a very heterogenous thickness and therefore an interval of values is shown. Table 2 summarizes the performance parameters of all the fabricated cells under solar-simulated AM 1.5 G illumination having an irradiance of 81–85 mW cm^{-2}. The curves obtained in dark conditions are shown in Figures S10 and S11 of Appendix A. The shunt (R_{sh}) and the series resistances (R_s) were determined from the inverse of the slopes of the *J-V* curves under illumination at the short condition ($V = 0$ V) and at the open circuit voltage, respectively.

The most efficient devices were based on the blends of PffBT4T-2OD:**PDI-Feo** (1:1.5) exhibiting a maximum PCE of 4.23%, a V_{OC} of 0.81 V, a J_{SC} of 10.92 mA cm^{-2} and a FF of 0.38. This PV performance is among the highest reported for PDI dimers [16,23,24] and establishes **PDI-Feo** among the first PDI-based acceptors with ethylene oxide solubilizing chains and noteworthy PV performance. A little larger PCE, of 4.96%, was reported by X. Zhang and *co*-workers for a thiophene-bridged PDI-dimer carrying both alkyl chains and two OE chains attached to the imide *N*-positions and to the bay positions respectively, after annealing treatments to the active layer [38]. The measured current density-voltage (*J-V*) curves and the External Quantum

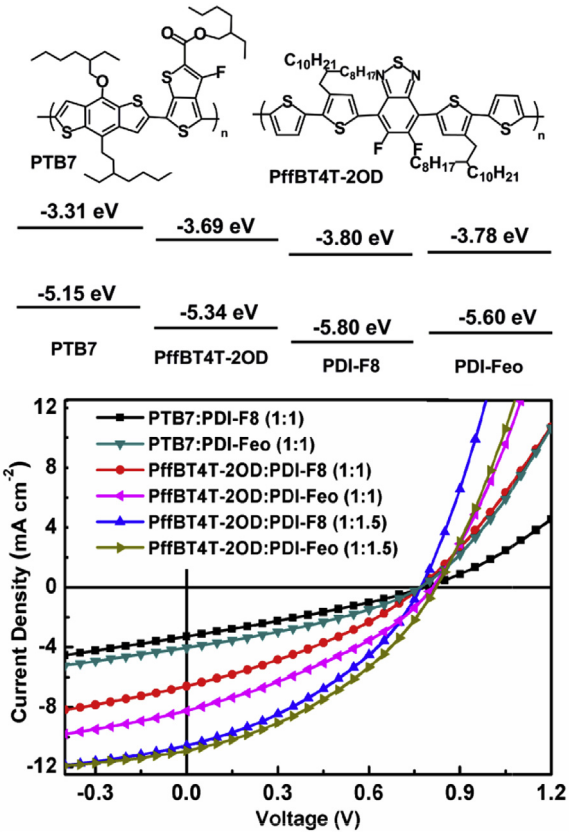

Fig. 3. OPV cells data. Chemical structure of the polymer donors used in this study, scheme of the energy levels determined by CV for the PDI dimers and from ref. 35 and ref. 36 for PffBT4T-2OD and PTB7, respectively and representative *J-V* curves obtained for the cells fabricated without DIO in the active layers.

efficiency spectra for the cells prepared without DIO in the active layer are shown in Figs. 3 and 4, respectively. The results for the series without DIO, more directly reflect the performance of PDIs alone in the cells. The EQE spectra in Fig. 4 show that both PDIs contribute to the photogenerated charges within the active layer with both polymer donors (spectra intensity in 400–500 nm range where polymers' absorption is low). As observed, for the cells without DIO, **PDI-F8** and **PDI-Feo** result in considerably different PV performance, with **PDI-Feo** based cells having larger J_{SC} and FF values for both polymer:PDI systems.

The improvement in PCE is of *ca.* 20% and 53% for cells with PffBT4T-2OD donor in 1:1.5 and 1:1 ratio, respectively, and *ca.* 28% for cells with PTB7 (1:1).

For the cells with PffBT4T-2OD, those with **PDI-Feo** also display considerably larger V_{OC} (0.81 V *vs.* 0.77 V). Differences in V_{OC} are usually explained in the light of the relation of V_{OC} with the difference between the HOMO of the donor and the LUMO of the acceptor [39]. Considering the similarity found between the estimated LUMO energies for the PDI dimers, we propose that within the blend with PffBT4T-

Table 2
Photovoltaic performance parameters of the fabricated PTB7:**PDI-F8** and PffBT4T-2OD:**PDI-Feo** based devices.

Active layer, D:A	V_{OC} (V)	J_{SC} (mA cm^{-2})	FF	PCE (%) best/ave[a]	AL Thickn. (nm)	R_{sh} (Ω cm^{-2})	R_s (Ω cm^{-2})
PTB7:PDI-F8, 1:1, 0% DIO	0.78	−3.29	0.29	0.88/0.83	125	289	150
PTB7:PDI-F8, 1:1, 1% DIO	0.77	−6.68	0.32	2.02/1.80	140	185	67
PTB7:PDI-F8, 1:1, 3% DIO	0.84	−5.22	0.43	2.23/2.10	125	706	98
PffBT4T-2OD:PDI-F8, 1:1, 0% DIO	0.77	−6.60	0.33	1.94/1.50	380–730	208	57
PffBT4T-2OD:PDI-F8, 1:1.5, 0% DIO	0.77	−10.57	0.37	3.55/3.09	190–340	204	26
PTB7:PDI-Feo, 1:1, 0% DIO	0.77	−4.04	0.33	1.21/1.06	100	312	75
PTB7:PDI-Feo, 1:1, 1% DIO	0.81	−4.29	0.39	1.67/1.37	125	523	85
PTB7:PDI-Feo, 1:1, 3% DIO	0.86	−3.24	0.46	1.49/1.09	125	932	83
PffBT4T-2OD:PDI-Feo, 1:1, 0% DIO	0.81	−8.25	0.34	2.83/2.29	310–430	189	37
PffBT4T-2OD:PDI-Feo, 1:1.5, 0% DIO	0.81	−10.92	0.38	4.23/3.71	140–170	241	29

[a] Best values followed by the averages calculated from 16 devices.

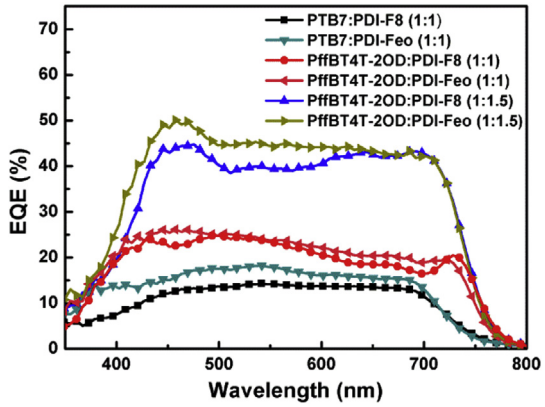

Fig. 4. External quantum efficiency (EQE) spectra. EQE as a function of the wavelength for the cells fabricated without DIO within the active layers.

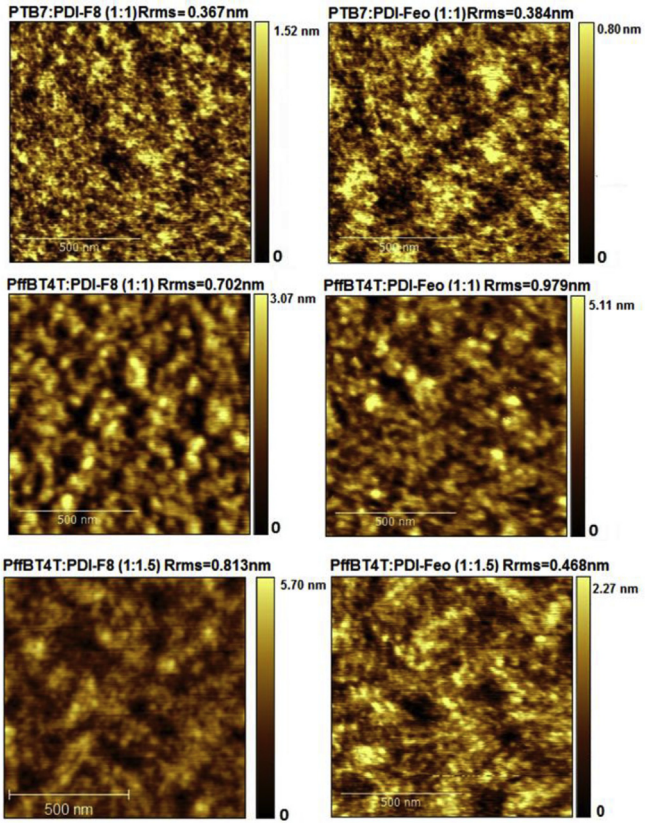

Fig. 5. Morphological characterization of active blends. AFM topographic images of the active layers of the cells fabricated without DIO.

2OD, **PDI-Feo** adopts a different conformation from that of **PDI-F8**, which affects its molecular orbital energies. We note that although the solubilizing chains do not contribute to the HOMO and LUMO levels of the PDIs, the assembly between the donor and the acceptor in the blend is determined by the intermolecular interactions between the two components and, therefore, it is affected by the nature of their solubilizing chains.

In the case of blends with PffBT4T-2OD, a different donor-acceptor assembly, caused by the different solubilizing chains of the PDIs and affecting their frontier molecular orbital energies, should therefore be present.

The surface analysis of these active layers by Atomic Force Microscopy (AFM) (Fig. 5) shows good film morphologies, with smooth surfaces and domains within the nanoscale (< 100 nm), and exhibit comparable characteristics, both in terms of roughness values and domain lateral sizes. Thus, it can be concluded that the proposed dissimilarity between the assembly of the PDIs with the PffBT4T-2OD donor should not alter significantly the phase separation in the blends and therefore it should be more related with different molecular conformations of the donor and/or the acceptor at their interface, provided by the distinct solubilizing chains of the PDIs. Regarding the cells with PTB7, a smaller variation in V_{OC} (0.01 V) is obtained, where the larger V_{OC} occurs for the blend with **PDI-F8**. Although of less importance, we suggest that, in this case, the variation in V_{OC} should also be caused by conformational variances in the intermolecular assemblies due to the different solubilizing chains of the PDI dimers.

The calculated series resistances for 1:1 blends are lower for **PDI-Feo** based cells when compared with the corresponding **PDI-F8** based cells, thus indicating that charge transport is more facilitated when **PDI-Feo** replaces **PDI-F8** within the blends. The better charge transport in blends with **PDI-Feo** can be the cause for the larger J_{SC} and FF values, since the molar extinction coefficients of the PDIs are equivalent and the active layers thicknesses are alike. Given that the morphologies of the active layers, as analyzed, do not show relevant dissimilarities, the difference in charge transport should be related to differences in intermolecular assembly at the inner scale, not detected by AFM. We suggest that in the case of **PDI-Feo**, a more densely packed π-π stacking between PDI dimers within the blend promoted by the more flexible EO chains, in comparison with alkyl chains, should be at the origin of a better charge transport for charge carriers within the **PDI-Feo** phase. This hypothesis agrees with the above-mentioned differences between the absorption spectra of the two PDI dimers in film, suggesting shorter distances of π-π stacking in the case of **PDI-Feo**. Another reason that can, at least in part, contribute to the larger J_{SC} obtained for cells with **PDI-Feo** is an enhancement in the relative dielectric constant, ε_r, of the **PDI-Feo**, in comparison with that of **PDI-F8**, favoring exciton dissociation. In fact, as referred (see Section 1), Torabi and *co*-workers [30] determined larger ε_r for a series of polymers and fullerene derivatives with EO side chains than for reference compounds carrying

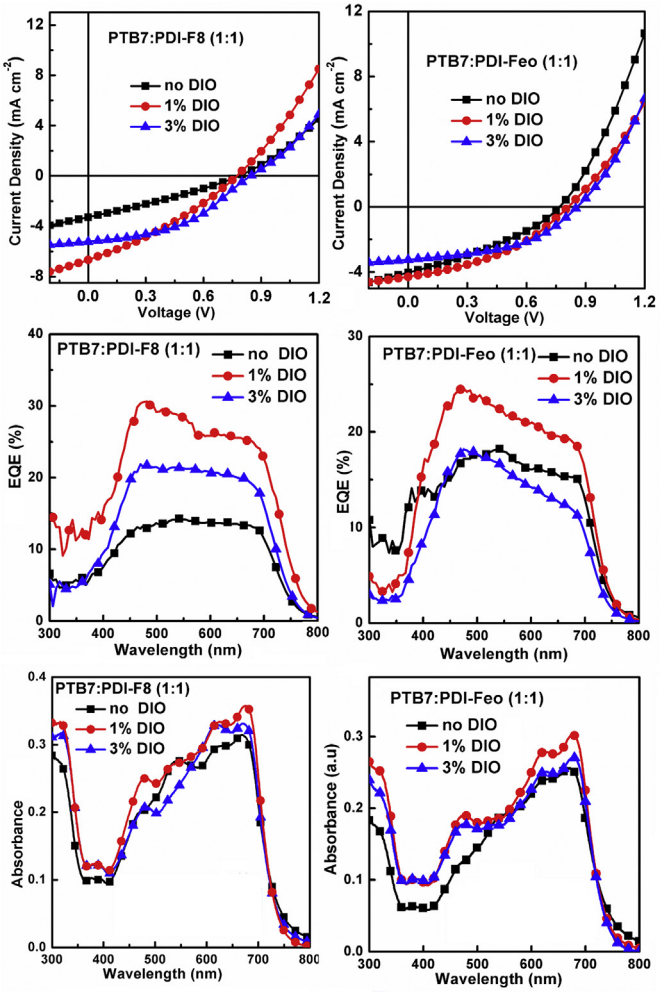

Fig. 6. OPV performance and blend absorption spectra of cells without DIO. Representative *J-V* curves, EQE, and absorption spectra for the cells fabricated with DIO in the active layers and comparison with analogous cells without DIO.

alkyl chains and proposed that the increased ε_r values can lead to reduced exciton binding regarding exciton lifetime and to improved charge generation within the donor-acceptor blends. These hypotheses of improved charge generation and/or transport within the blends with **PDI-Feo** are in accordance with the EQE spectra in Fig. 4 showing higher intensity in the PDIs contribution range (400–550 nm) for the **PDI-Feo**-based cells than for the corresponding cells with **PDI-F8**.

3.4.1. The effect of DIO in PTB7:PDI dimers-based OSCs

To further optimize the performance of the fabricated cells, the additive 1,8-diiodooctane was used in low contents within the blend solutions of PTB7:PDI dimers. For the PffBT4T-2OD-based cells, the blend solutions yielded very heterogeneous films and resulted in cells with very poor efficiencies (< 0.4%) (results not shown). Fig. 6 shows representative *J-V* curves, EQE (%), and absorption spectra of the fabricated cells with DIO and comparison with the reference cells without DIO. The PV performance of the cells is shown in Table 2.

For both blends, PTB7:**PDI-F8** and PTB7:**PDI-Feo** blends, the addition of 1% of DIO caused increased J_{SC} and FF values, while the further increase to 3% in DIO caused a decrease in J_{SC} but a significant raise in FF (from 0.32 to 0.43 in PTB7:**PDI-F8** blends and from 0.39 to 0.46 in PTB7:**PDI-Feo** blends). However, the interplay between the PV parameters implies that no further improvement resulted from incrementing DIO from 1% to 3% in the cells with PTB7:**PDI-Feo** blends. The EQE spectra for cells with DIO display increased relative intensity in the PDI contribution range (400–550 nm) therefore indicating that when DIO is added, both PDI dimers are favourably affected regarding their capability to contribute to PV operation. One hypothesis is that DIO, due to better dissolving the PDI dimer than the polymer and its higher T_b than that of the main solvent (T_b of CB is 131 °C and of DIO is 332.5 °C), allows the PDI dimer to self-organize in the dimer-DIO liquid phase after the polymer precipitates and form stacks with shorter π-π distances where charge transport is facilitated. In fact, analysis of 2D grazing-incidence X-ray diffraction (GIXRD) on polymer:PDI-dimer blends prepared from o-dichorobenzene, also showing an improvement in PV performance upon addition of small contents of DIO, demonstrated more ordered packing of the PDI dimers [40]. Considering the absorption spectra for the PTB7:**PDI-F8**-based cells, the addition of DIO results in a reduction of the relative intensity of the peak at 550 nm while for the PTB7:**PDI-Feo** based cells a reduction in the peak at 473 nm is observed. However, the peak positions are not affected with the addition of DIO. These results are in contrast with other studies that show significant shifts of the absorption peaks of PDI monomeric acceptors in donor-acceptor blend films [41]. In such studies, higher contents of DIO led to red shifts in the PDI absorption peaks, indicative of large *J-J*-aggregates, whereas lower contents (0.4%) caused blue shifts (*H*-aggregation). In our blends, as no differences in the peaks positions are observed, even with the higher DIO content, we conclude that **PDI-F8** and **PDI-Feo** do not form undesirable large aggregates in blend films, due to their twisted conformations. The spectral changes observed when DIO is added are possibly associated to the conformational modifications of the PDIs when they self-organize within the DIO-PDI phase.

The blends of the films prepared with DIO as co-solvent were also analyzed by AFM. The topography images for such blends (Fig. 7) reveal less smooth surfaces than those of the reference blends without DIO, and larger domains sizes. The corresponding phase images (Fig. S12 in Appendix A) seem to indicate that in the case of PTB7:**PDI-Feo** blends the surface is mostly composed of the same component. In the case of PTB7:**PDI-F8** blends with 1% DIO, both components seem to be more equally distributed, whereas a more heterogenous surface phase is shown for the 3% DIO case. Given that the blends only differ in the PDI-dimer, we therefore conclude that the hydrophilic ethylene oxide groups can affect the vertical phase separation within the D:A blend.

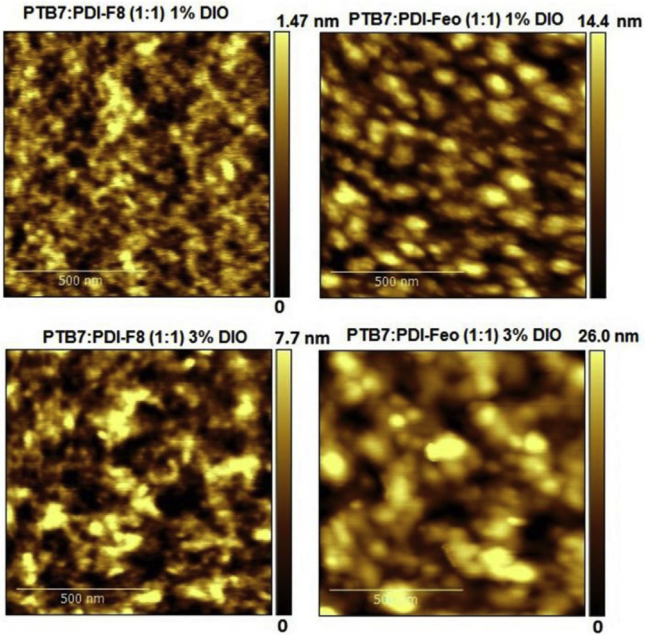

Fig. 7. AFM topographic images of the active layers of the cells fabricated with DIO.

Since the shunt resistances for PTB7:**PDI-Feo** based cells with DIO (Table 2) are large, therefore indicating less losses caused by bimolecular recombination, we suggest that **PDI-Feo** is partially segregated at the blend surface and consequently reduces bimolecular recombination at the interface with the electron-collector electrode. Considering the improved PV performance of the blends with DIO, the observed morphological modifications appear to favour PV operation, however, further investigations should be carried out to better understand the role of DIO in the cells.

4. Conclusions

Two new PDI dimers with a fluorene bridge unit were synthesized and investigated and the results showed that solubilizing chains based on ethylene oxide (EO) groups anchored to the fluorene unit lead to improved OSCs performance in comparison with alkyl chains, while not noticeably affecting the optoelectronic properties of PDI-based acceptors. Both PDI dimers have twisted conformations towards the bridge units, thereby preventing the formation of large aggregates which are typically detrimental for PV operation. Differences in the intermolecular organization, promoted by the more flexible EO chains and causing closer π-π stacking in PDI intermolecular assemblies, are suggested to be the main cause for the observed improved PV performance obtained for the PDI modified with EO chains. The OSCs based on one of the tested polymer donors, PTB7, were further optimized by using 1,8-diiodooctane in low contents (1–3%) as additive in the solvent. In conclusion, this work provides new insights into the molecular design of PDI dimers, one of the most attractive non-fullerene family of acceptors for OSCs.

Acknowledgments

This work was supported by Fundação para a Ciência e a Tecnologia (FCT-portugal) (contract no. UID/EEA/50008/2013), Ministerio de Economía, Industria y Competitividad of Spain (contracts no. CTQ2014-55798-R and no. CTQ2017-87102-R), Generalitat Valenciana (contract no. APOSTD17). The authors also thank to the networking support by the COST Action MP1307 StableNextSol.

Appendix A. Supplementary data

Supplementary data to this article can be found online at https://doi.org/10.1016/j.dyepig.2018.09.051.

References

[1] Heeger AJ. Semiconducting polymers: the third generation. Chem Soc Rev 2010;39:2354–71. https://doi.org/10.1039/b914956m.
[2] Søndergaard R, Hosel M, Angmo D, Larsen-Olsen TT, Krebs FC. Roll-to-roll fabrication of polymer solar cells. Mater Today 2012;15:36–49https://doi.org/10.1016/S1369-7021(12)70019-6.
[3] Sumaiya S, Kardel K, El-Shahat A. Organic solar cell by inkjet printing—an overview. Technologies 2017;5:53https://doi.org/10.3390/technologies5030053.
[4] Youn H, Park HJ, Guo LJ. Organic photovoltaic cells: from performance improvement to manufacturing processes. Small 2015;11:2228–46https://doi.org/10.1002/smll.201402883.
[5] Zhao W, Li S, Yao H, Zhang S, Zhang Y, Yang B, et al. Molecular optimization enables over 13% efficiency in organic solar cells. J Am Chem Soc 2017;139:7148–51. https://doi.org/10.1021/jacs.7b02677.
[6] Zhao J, Li Y, Yang G, Jiang K, Lin H, Ade H, et al. Efficient organic solar cells processed from hydrocarbon solvents. Nat Energy 2016;1:15027https://doi.org/10.1038/nenergy.2015.27.
[7] Fei Z, Eisner FD, Jiao X, Azzouzi M, Röhr JA, Han Y, et al. Surpassing 10% efficiency benchmark for nonfullerene organic solar cells by scalable coating in air from single nonhalogenated solvent. Adv Mater 2018;30:1705485https://doi.org/10.1002/adma.201705485.
[8] Ebenhoch B, Thomson SAJ, Genevičius K, Juška G, Samuel IDW. Charge Carrier mobility of the organic photovoltaic materials PTB7 and PC71BM and its influence on device performance. Org Electron 2015;22:62–8https://doi.org/10.1016/j.orgel.2015.03.013.
[9] Abramavicius V, Pranculis V, Melianas A, Inganäs O, Gulbinas V, Abramavicius D. Role of coherence and delocalization in photo-induced electron transfer at organic interfaces. Sci Rep 2016;6:32914. https://doi.org/10.1038/srep32914.
[10] Vithanage DA, Devižis A, Abramavičius V, Infahsaeng Y, Abramavičius D, MacKenzie RCI, et al. Visualizing charge separation in bulk heterojunction organic solar cells. Nat Commun 2013;4:2334. https://doi.org/10.1038/ncomms3334.
[11] Tournebize A, Bussière P-O, Rivaton A, Gardette JL, Medlej H, Hiorns RC, et al. New insights into the mechanisms of photodegradation/stabilization of P3HT:PCBM active layers using poly(3-hexyl-d13-thiophene). Chem Mater 2013;25:4522–8. https://doi.org/10.1021/cm402193y.
[12] He Y, Chen H-Y, Hou J, Li Y. Indene−C60 bisadduct: a new acceptor for high-performance polymer solar cells. J Am Chem Soc 2010;132:1377–82. https://doi.org/10.1021/ja908602j.
[13] Zhong Y, Trinh MT, Chen R, Purdum GE, Khlyabich PP, Sezen M, et al. Molecular helices as electron acceptors in high-performance bulk heterojunction solar cells. Nat Commun 2015;6:8242https://doi.org/10.1038/ncomms9242.
[14] Sun D, Meng D, Cai Y, Fan B, Li Y, Jiang W, et al. Non-fullerene-acceptor-based bulk-heterojunction organic solar cells with efficiency over 7%. J Am Chem Soc 2015;137:11156–62. https://doi.org/10.1021/jacs.5b06414.
[15] Fernández-Lázaro F, Zink-Lorre N, Sastre-Santos Á. Perylenediimides as non-fullerene acceptors in bulk-heterojunction solar cells (BHJSCs). J Mater Chem A 2016;4:9336–46. https://doi.org/10.1039/C6TA02045C.
[16] Yan Q, Zhou Y, Zheng Y-Q, Pei J, Zhao D. Towards rational design of organic electron acceptors for photovoltaics: a study based on perylenediimide derivatives. Chem Sci 2013;4:4389–94. https://doi.org/10.1039/C3SC51841H.
[17] Weitz RT, Amsharov K, Zschieschang U, Villas EB, Goswami DK, Burghard M, et al. Organic n-channel transistors based on core-cyanated perylene carboxylic diimide derivatives. J Am Chem Soc 2008;130:4637–45. https://doi.org/10.1021/ja074675e.
[18] Meng D, Sun D, Zhong C, Liu T, Fan B, Huo L, et al. High-performance solution-processed non-fullerene organic solar cells based on selenophene-containing perylene bisimide acceptor. J Am Chem Soc 2016;138:375. https://doi.org/10.1021/jacs.5b11149.
[19] Hendsbee AD, Sun JP, Law WK, Yan H, Hill IG, Spasyuk DM, et al. Synthesis, self-assembly, and solar cell performance of N-annulated perylene diimide non-fullerene acceptors. Chem Mater 2016;28:7098–109. https://doi.org/10.1021/acs.chemmater.6b03292.
[20] Jiang W, Ye L, Li X, Xiao C, Tan F, Zhao W, et al. Bay-linked perylene bisimides as promising non-fullerene acceptors for organic solar cells. Chem Commun 2014;50:1024–6. https://doi.org/10.1039/C3CC47204C.
[21] Yan Q, Zhou Y, Zheng Y-Q, Pei J, Zhao D. Towards rational design of organic electron acceptors for photovoltaics: a study based on perylenediimide derivatives. Chem Sci 2013;4:4389–94. https://doi.org/10.1039/C3SC51841H.
[22] Yu Y, Yang F, Ji Y, Wu Y, Zhang A, Li C, et al. A perylene bisimide derivative with a LUMO level of −4.56 eV for non-fullerene solar cells. J Mater Chem C 2016;4:4134–7. https://doi.org/10.1039/C6TC01045H.
[23] Hartnett PE, Matte HSSR, Eastham ND, Jackson NE, Wu Y, Chen LX, et al. Ring-fusion as a perylenediimide dimer design concept for high-performance non-fullerene organic photovoltaic acceptors. Chem Sci 2016;7:3543–55. https://doi.org/10.1039/C5SC04956C.
[24] Stenta C, Molina D, Viterisi A, Montero-Rama MP, Pla S, Cambarau W, et al. Diphenylphenoxy-thiophene-pdi dimers as acceptors for OPV applications with open circuit voltage approaching 1 Volt. Nanomaterials 2018;8:211https://doi.org/10.3390/nano8040211.
[25] Sun J-P, Hendsbee AD, Dobson AJ, Welch GC, Hill IG. Perylene diimide based all small-molecule organic solar cells: Impact of branched-alkyl side chains on solubility, photophysics, self-assembly, and photovoltaic parameters. Org *Electron* 2016;35:151–7https://doi.org/10.1016/j.orgel.2016.05.012.
[26] Sengwa RJ. Solvent effects on microwave dielectric relaxation in poly(ethylene glycols). Polym Int 1998;45:43–6. https://doi.org/10.1002/(SICI)1097-0126(199801)45:1 < 43::AID-PI902 > 3.0.CO;2-1.
[27] Lei T, Wang J-Y, Pei J. Roles of flexible chains in organic semiconducting materials. Chem Mater 2014;26:594–603. https://doi.org/10.1021/cm4018776.
[28] Kanimozhi C, Yaacobi-Gross N, Chou KW, Amassian A, Anthopoulos TD, Patil S. Diketopyrrolopyrrole–diketopyrrolopyrrole-based conjugated copolymer for high-mobility organic field-effect transistors. J Am Chem Soc 2012;134:16532–5. https://doi.org/10.1021/ja308211n.
[29] Chen Y, Zhang S, Wu Y, Hou J. Molecular design and morphology control towards efficient polymer solar cells processed using non-aromatic and non-chlorinated solvents. Adv Mater 2014;26:2744–9. https://doi.org/10.1002/adma.201304825.
[30] Torabi S, Jahani F, Severen IV, Kanimozhi C, Patil S, Havenith RWA, et al. Strategy for enhancing the dielectric constant of organic semiconductors without sacrificing charge Carrier mobility and solubility. Adv Funct Mater 2015;25:150–7https://doi.org/10.1002/adfm.201402244.
[31] Chen X, Zhang Z, Ding Z, Liu J, Wang L. Diketopyrrolopyrrole-based conjugated polymers bearing branched oligo(ethylene glycol) side chains for photovoltaic devices. Angew Chem Int Ed 2016;55:10376–80. https://doi.org/10.1002/anie.201602775.
[32] Hou Q, Xu Y, Yang W, Yuan M, Peng J, Cao Y. Novel red-emitting fluorene-based copolymers. J Mater Chem 2002;12:2887–92. https://doi.org/10.1039/B203862E.
[33] Wang H, Chen L, Zha Z, Xiao Y. Aryl-bisalkynyl bridged perylene diimides dimers: efficient synthesis, properties and improved electron mobilities. Dyes Pigments 2017;144:184–9https://doi.org/10.1016/j.dyepig.2017.05.030.
[34] Meng B, Song H, Chen X, Xie Z, Liu J, Wang L. Replacing alkyl with oligo(ethylene glycol) as side chains of conjugated polymers for close π–π stacking. Macromolecules 2015;48:4357–63. https://doi.org/10.1021/acs.macromol.5b00702.

[35] Liu Y, Zhao J, Li Z, Mu C, Ma W, Hu H, et al. Aggregation and morphology control enables multiple cases of high-efficiency polymer solar cells. Nat Commun 2014;5:5293https://doi.org/10.1038/ncomms6293.
[36] He Z, Zhong C, Su S, Xu M, Wu H, Cao Y. Enhanced power-conversion efficiency in polymers solar cells using an inverted structure. Nat Photon 2012;6:591–5. https://doi.org/10.1038/srep17329.
[37] Xie S, Zhang J, Wu L, Zhang J, Li C, Chen X, et al. Vinylene- and ethynylene-bridged perylene diimide dimers as nonfullerene acceptors for polymer solar cells. Dyes Pigments 2017;146:143–50https://doi.org/10.1016/j.dyepig.2017.06.049.
[38] Zhang X, Li W, Yao J, Zhan C. High-efficiency nonfullerene polymer solar cell enabling by integration of film-morphology optimization, donor selection, and interfacial engineering. ACS Appl Mater Interfaces 2016;8:15415–21. https://doi.org/10.1021/acsami.6b03926.
[39] Scharber MC, Mühlbacher D, Koppe M, Denk P, Waldauf C, Heeger AJ, et al. Design rules for donors in bulk-heterojunction solar cells—towards 10 % energy-conversion efficiency. Adv Mater 2006;18:789–94https://doi.org/10.1002/adma.200501717.
[40] Lu Z, Jiang B, Zhang X, Tang A, Chen L, Zhan C, et al. Perylene–Diimide based nonfullerene solar cells with 4.34% efficiency through engineering surface donor/acceptor compositions. Chem Mater 2014;26:2907–14. https://doi.org/10.1021/cm5006339.
[41] Namepetra A, Kitching E, Eftaiha AF, Hill IG, Welch GC. Understanding the morphology of solution processed fullerene-free small molecule bulk heterojunction blends. Phys Chem Chem Phys 2016;18:12476. https://doi.org/10.1039/C6CP01269H.